Electronic Supplementary Material (ESI) for Journal of Materials Chemistry C.

SUPPLEMENTARY INFORMATION

Revisiting Syntheses of Fe_3O_4 Nanoparticles in Water and Lower Alcohols for Memristive Application

Mariia A. Mikhailova,[a] Ivan Yu. Chernyshov,[a,b] Georgii A. Illarionov,[a] Denis S. Kolchanov,[a] Oleg A. Kuchur,[a] Alexandr V. Vinogradov,[a] Sofia M. Morozova,[a,c] and Maxim I. Morozov [a*]

[a.] *Laboratory of Solution Chemistry of Advanced Materials and Technologies, ITMO University, Lomonosova str. 9, St.Petersburg, 191002, Russian Federation.*
[b.] *Inorganic Systems Engineering Group, Delft University of Technology, Van der Maasweg 9, 2629 HZ Delft, The Netherlands*
[c.] *N. E. Bauman Moscow State Technical University, 5 Baumanskaya 2-ya St., Moscow, 105005, Russian Federation*
* Corresponding author. E-mail: morozov@scamt-itmo.ru

1. Synthesis of iron oxide NPs in lower alcohols

Magnetite (Mt) nanoparticles (NPs) were obtained by the solvothermal method using $Fe(AcAc)_3$ as an iron-containing precursor and lower alcohols as organic solvents. The scheme is illustrated in Fig. S1. The optimal synthesis condition was found experimentally for *i*-PrOH, as listed in Table S1, and then remained unchanged for other lower alcohols.

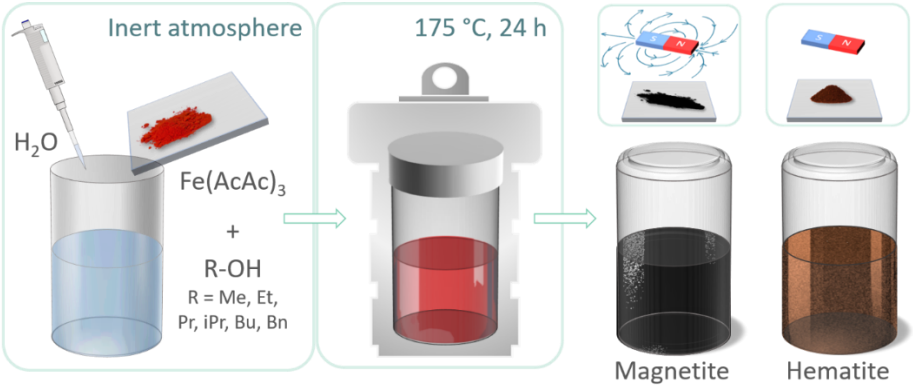

Fig. S1 Scheme of solvothermal synthesis of iron oxides in lower alcohols.

Table S1. Synthesis conditions and features of the resulting products for the synthesis of iron oxides in isopropyl alcohol.

Temperature (°C)	Time (h)	Heating rate (°C·min^{-1})	Precursors ratio Fe(AcAc)$_3$/*i*-PrOH (g·ml^{-1})	Appearance	Magnetic response
70	48	1.7	0.2/15	Red-brown dispersion	No
150	6	1.4	0.2/15	Red-brown dispersion	No
	12	0.8	0.1/20	Red-brown dispersion	No
175	12	1.0	0.05/15	Red-brown liquid	No
	12	1.7	0.1/7.5	Red-brown dispersion	Yes
	12	1.0	0.1/10	Black precipitate	Yes
	24	1.0	0.2/15	Black precipitate	Yes
	24	1.7	0.2/15	Black precipitate	Yes

2. Functional inks and thin films

For the magnetite nanoparticles obtained by the hydrolytic synthesis, the functional inks were experimentally optimized by diluting the experimentally obtained 4 wt.% Fe_3O_4 hydrosol with methanol and taking into accont the rheological property and stability of the colloidal system, as illustrated in Fig. S2a. For the non-hydrolytically synthesized magnetite, the functional ink was obtained by redispersion in methanol at a concentration of 0.04 wt.% that corresponds to the optimal colloidal stability, as illustrated in Fig. S2b. Fig. S3 illustrates AFM images of the scratched area in thin films fabricated using hydrolytic (Fig. S3a) and non-hydrolytic (Fig. S3b) Fe_3O_4 inks adopted for evaluation of their thickness.

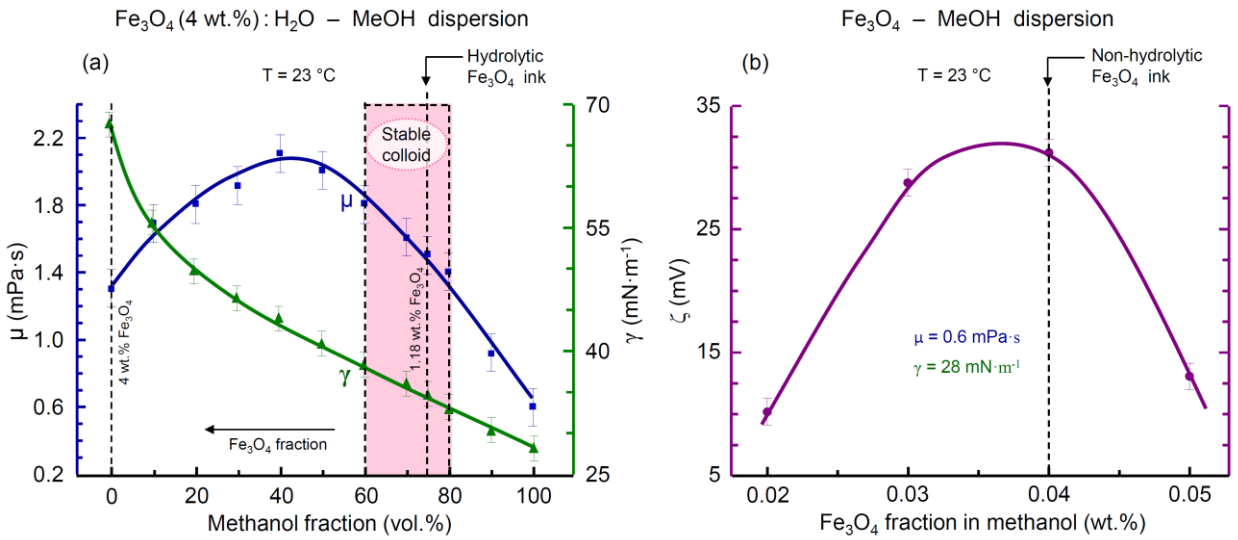

Fig. S2 (a) Viscosity (μ) and surface tension (γ) for a colloidal system consisting of 4 wt.% Fe_3O_4 hydrosol diluted with methanol. The highlighted area corresponds to high colloidal stability. (b) ζ-potential for non-hydrolytically synthesized Fe_3O_4 nanoparticles dispersed in methanol.

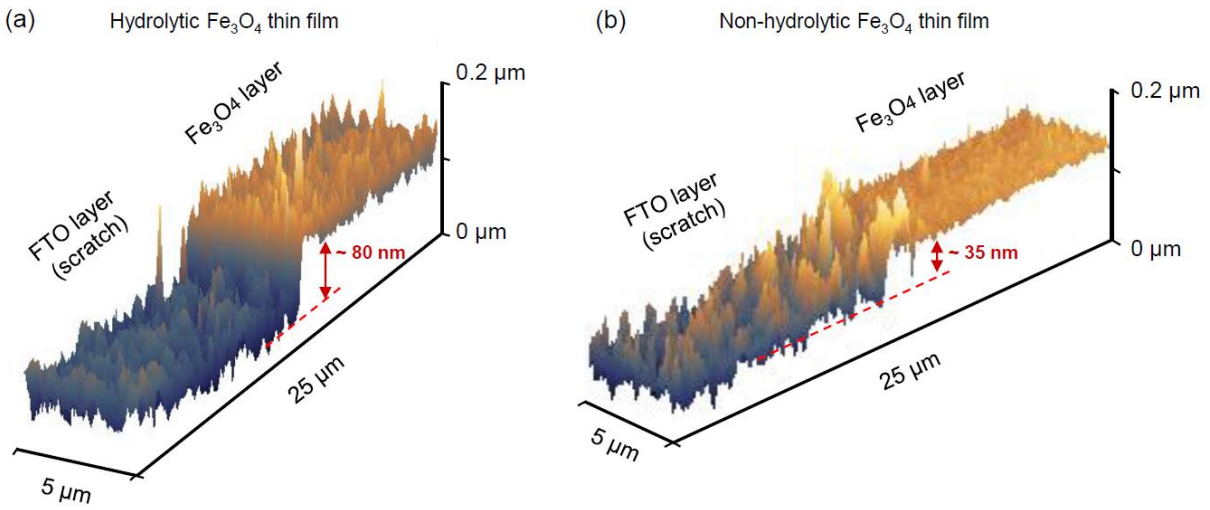

Fig. S3 AFM images of scratched surfaces for thin films fabricated using (a) hydrolytic and (b) non-hydrolytic Fe_3O_4 inks and evaluation of their thickness.

3. Phase analysis

A preliminary phase identification was performed using visual analysis of the color and magnetic response (Fig. S1). The color manifestations of all the obtained powder products were of the following three types, as illustrated in Fig. S4: dark (Fig. S4a), red-brown (Fig. S4b), and dark-brown (Fig. S4c), which in combination with XRD analysis have been attributed to magnetite, hematite, and various mixed phases of magnetite with crystalline or amorphous iron(III) oxide, correspondingly.

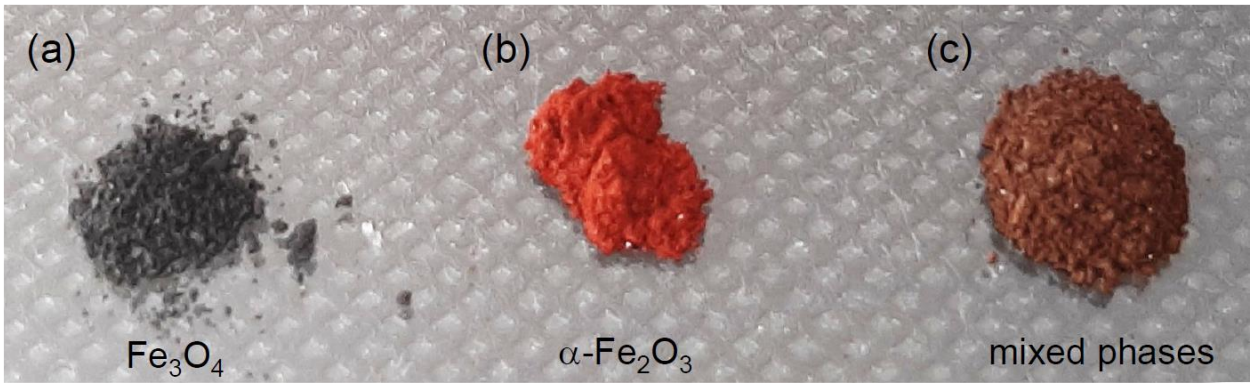

Fig. S4 Color manifestation of iron oxide nanopowders obtained in the study: (a) magnetite; (b) hematite; (c) mixture of Fe_3O_4 and Fe_2O_3 phases.

Fig. S5 depicts an extended XRD pattern for the synthesized products in MeOH at 175 °C. Besides the reflexions attributed to iron oxides α-Fe_2O_3 and Fe_3O_4, a series of unidentified peaks suggests a multiphase mixture of intermediate products indicating incomplete synthesis reactions. In particular, a low-angle peak corresponding to an interatomic plane distance of *ca.* 9.89 Å may indicate the presence of intermediate metal-organic products such as iron methoxide[S1] and/or acetatates.[S2] A list of reference phases used for the peaks identification is presented in Table S2.

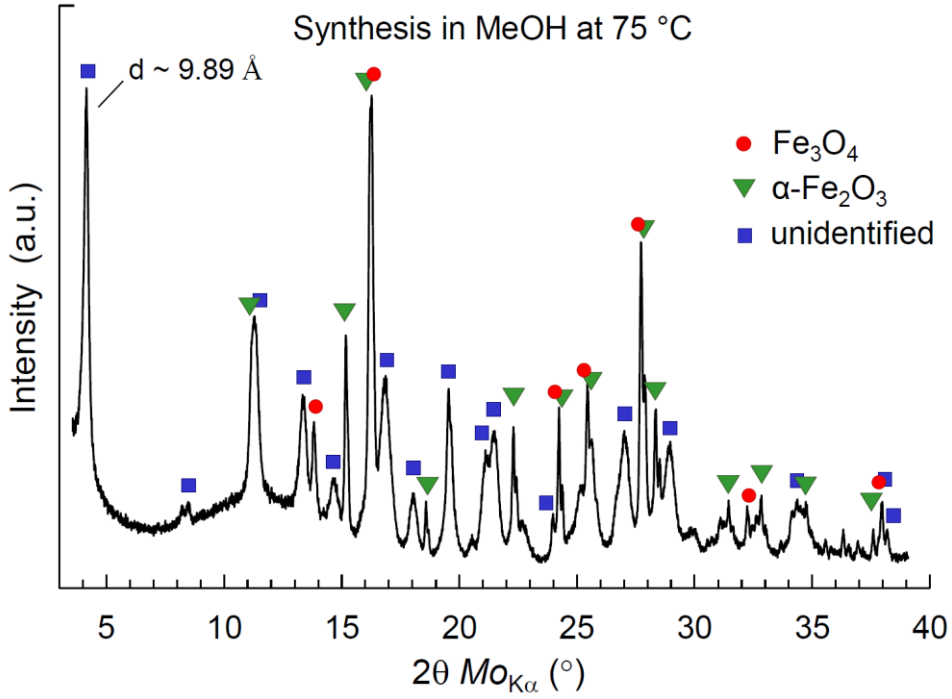

Fig. S5 XRD pattern for profucts synthesized in MeOH at 175° C

Table S2. References used for XRD phase identification of the solvothermal synthesis products obtained in MeOH at 175 °C.

Compound	Database, reference ID	Presence
α-Fe_2O_3 (hematite)	JCPDS PDF: 000-33-0664	detected
Fe_3O_4 (iron oxide)	JCPDS PDF: 000-19-0629	detected
γ-Fe_2O_3 (maghemite)	JCPDS PDF: 000-39-1346	not excluded
FeO (wüstite)	JCPDS PDF: 000-89-7100	not detected
$FeCO_3$ (siderite)	JCPDS PDF: 000-29-0696	not detected
$Fe_2O_2CO_3$ (iron oxycarbonate)	JCPDS PDF: 000-33-0665	not detected
$Fe(C_5H_7O_2)_3$ (iron(III) acetylacetonate)	JCPDS PDF: 000-30-1763	not detected
$Fe(C_5H_7O_2)_2$ (iron(II) acetylacetonate)	JCPDS PDF: 000-30-1762	not detected
$Fe(CH_3COO)_3$ (iron(III) acetate)	CCDC code: HIHXOM	not excluded

$Fe(CH_3COO)_2$ (iron(II) acetate)	CCDC code: QQQFUY01	not excluded
$Fe(OCH_3)_3$ (iron methoxide)	JCPDS PDF: 000-45-1510	not excluded
$Fe(OH)_3$ (iron hydroxide)	JCPDS PDF: 000-38-0032	not detected
FeOOH (goethite)	JCPDS PDF: 000-29-0713	not detected
FeOOH (lepidocrocite)	JCPDS PDF: 000-44-1415	not detected

2. Influence of water addition on synthesis iron oxide NP in *i*-PrOH.

Investigation of water influence on the synthesis of iron oxide from $Fe(AcAc)_3$ in *i*-PrOH at 175 °C has been provided for varios water content in the range 0.3 – 0.8 wt.%. The results of phase analysis of the synthesized products by the means of XRD characterization are shown in Fig. S6.

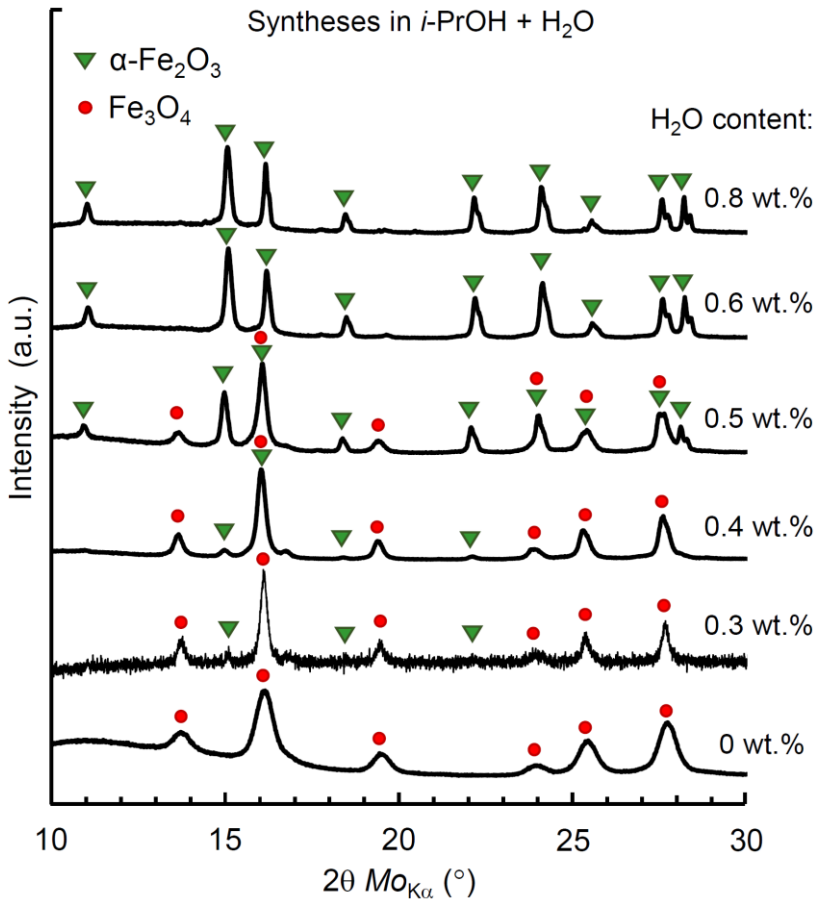

Fig. S6 XRD patterns for iron oxides NPs synthesized at 175° C for 24 h in i-PrOH with various amount of water.

3. Theoretical modeling

For comparison of alcohol-driven Fe^{3+}/Fe^{2+} reduction rates, transition states of the hydrogen transfer from alcohol to Fe^{3+}–O–Fe^{3+} moiety were calculated. Fe^{3+}–O–Fe^{3+} moiety was modeled as a binuclear iron complex with 3 malondialdehyde anions, 2 methanol molecules, and alcoholate anion (Fig. S7a). Methanol molecules and malondialdehyde anions were used to simplify the calculation system. For the alcohol dehydration process, an S_N2 reaction between alcohol and protonated alcohol was calculated (Fig. S7b). Activation energies were estimated as a difference in energies between the transition state and distinct reagents. The results with and without correction on the solvation effect by the corresponding alcohols are listed in Table S3.

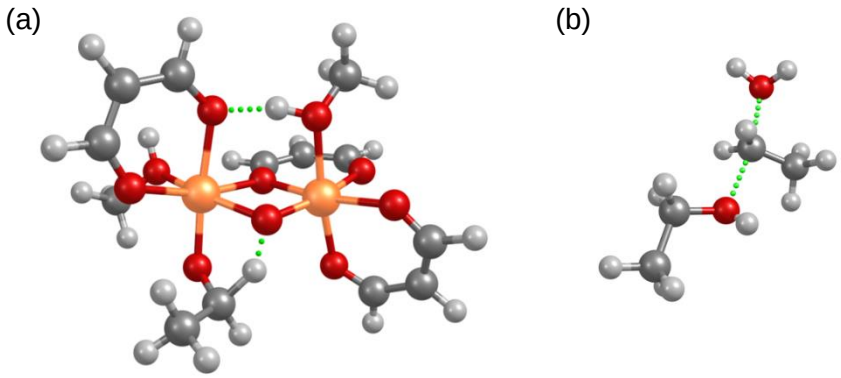

Fig. S7 Localized transition states for the models addressing (a) Fe^{3+}/Fe^{2+} reduction and (b) dehydration to ether processes exemplified on ethanol.

Table S3. Activation energies of the considered reactions, kJ/mol.

Alcohol	Fe^{3+}/Fe^{2+} reduction		Dehydration	
	E_a^{PCM} a)	$E_a^{COSMO\text{-}RS}$ b)	E_a^{PCM} a)	$E_a^{COSMO\text{-}RS}$ b)
MeOH	103.4	106.9	34.3	34.5
EtOH	102.7	102.7	34.3	34.3
n-PrOH	103.0	99.6	32.3	32.0
i-PrOH	96.3	98.7	30.6	30.3
n-BuOH	104.7	100.8	31.9	31.4
i-BuOH	104.5	102.6	34.8	34.3
BnOH	81.2	78.2	15.0	14.1

a) Activation energies, calculated from PCM electronic energies in EtOH.

b) Activation energies with COSMO-RS correction on solvation by the corresponding alcohol.

4. Synthesis of iron oxide NPs in BnOH

Investigation of lowering temperature effect on the synthesis of iron oxide from $Fe(AcAc)_3$ in BnOH was performed at a reference temperature of 175 °C [S3] and at a lower temperature of 150 °C, just a few degree below the decomposition temperature reported for $Fe(AcAc)_3$.[S4] The results of phase analysis of the synthesized products by the means of XRD characterization are shown in Fig. S8. Despite of an identical single phase crystalline product identified as magnetite has been observed in both cases, the difference in samples color suggests that NPs synthesized at 150 °C contain an additional non-reduced iron oxide product, most likely, an amorphous phase.

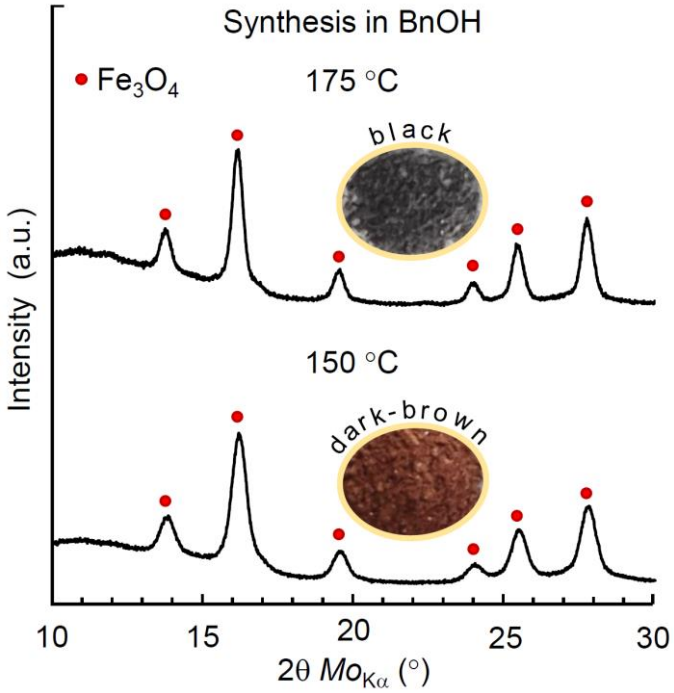

Fig. S8 XRD patterns for iron oxides NPs synthesized at 175° C for 24 h in *i*-PrOH with various amount of water.

5. Characterization of Mt NPs obtained by hydrolytic and non-hydrolytic routes.

Examination of phase purity for the product obtained by the hydrolytic and non-hydrolytic (*i*-PrOH, 175 °C) synthesis routes was performed by XRD. The corresponding patterns are shown in Fig. S9. Only Mt phase has been detected in both samples, which also corresponds to their black color (Fig. S4a). The surface morphology of magnetite samples obtained by the hydrolytic and nonhydrolytic (i-PrOH) syntheses was characterized by the means of SEM and gas adsorption-desorption isotherms using BET and BJH analyses. The experimental results are shown in Fig. S10a,b and Fig. S11a,b, correspondingly. Magnetization curves for the both cases are illustrated in Fig. S12. Mt NPs obtained in *i*-PrOH, 175 °C showed a lower saturation level of the specific magnetization (*ca.* 46 emu·g^{-1}) compared to the previously reported value for Mt NP obtained by the hydrolytic route (*ca.* 88 emu·g^{-1}).[S5] Fig. S13 illustrates the time profiles of the driving voltage (Fig. S13a), current response (Fig. S13b) and the corresponding resistance (Fig. S13c) measured during the electrical characterization of a hydrolytically obtained Fe_3O_4 thin film. The corresponding low-signal voltage-current relationships are shown in Fig. S13d and Fig. S13e for the high-resistace and low-resistance states, respectively.

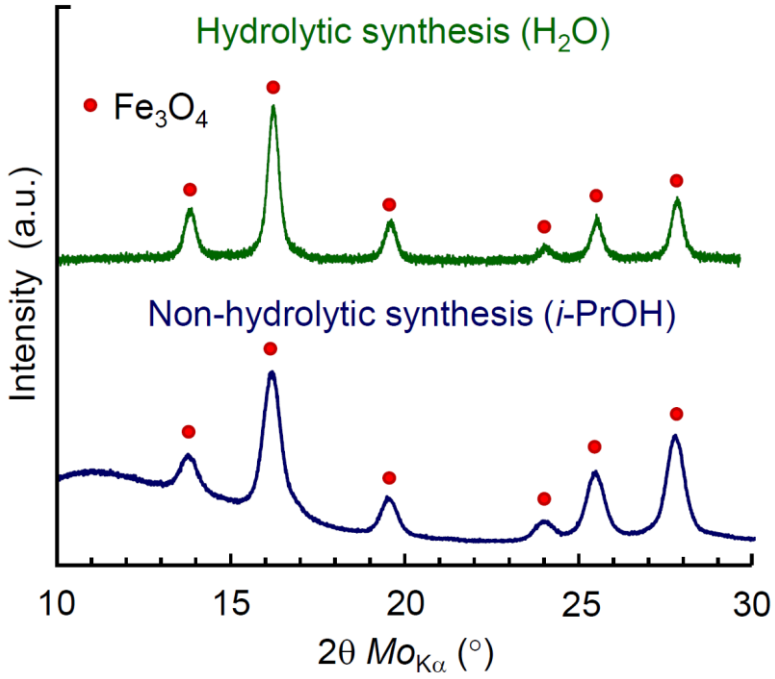

Fig. S9 XRD patterns for iron oxides NPs prepared by hydrolytic synthesis and by synthesis in i-PrOH at 175° C.

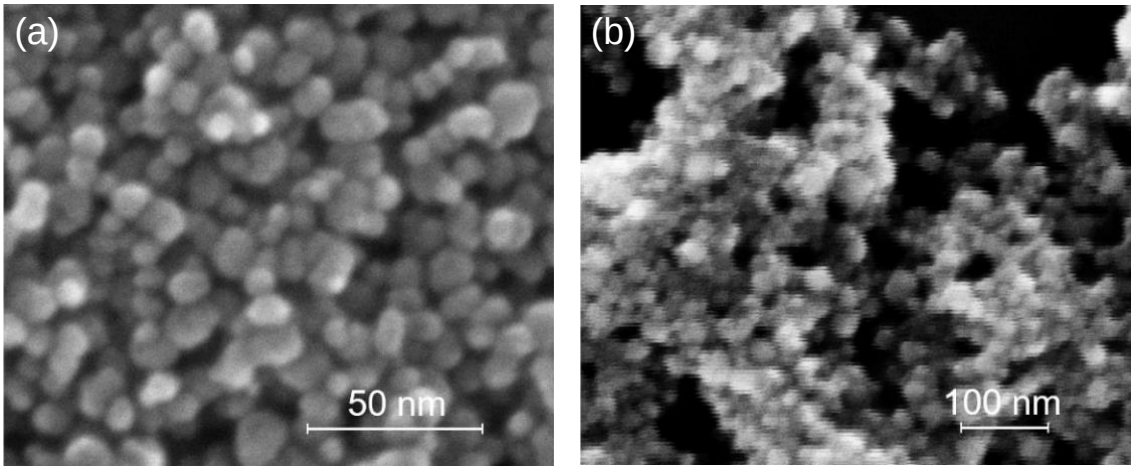

Fig. S10 SEM images of magnetite NPS obtained by (a) hydrolytic and (b) nonhydrolytic (i-PrOH) synthesis routes.

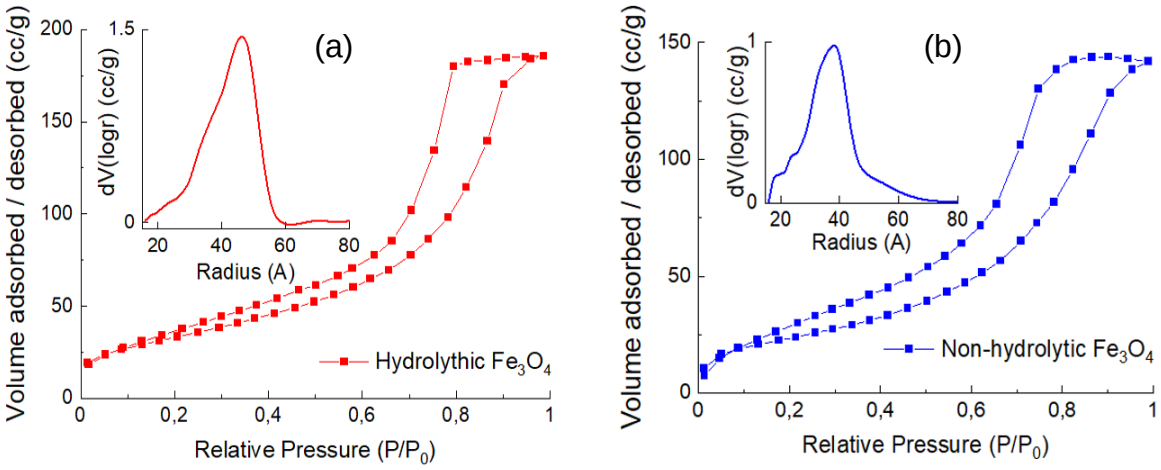

Fig. S11 Nitrogen gas adsorption-desorption isotherms for magnetite NPS obtained by (a) hydrolytic and (b) nonhydrolytic (i-PrOH) synthesis routes.

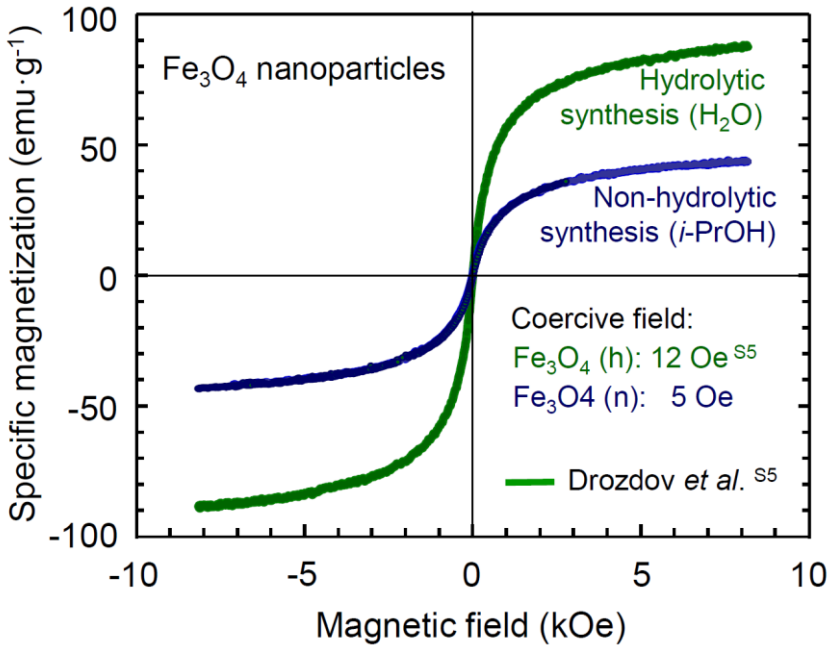

Fig. S12 Magnetization curves for magnetite nanoparticles prepared by hydrolytic and non-hydrolytic (i-PrOH, 175 °C) routes. The data for Mt NPs obtained by the hydrolytic synthesis are adopted from ref.[S5]

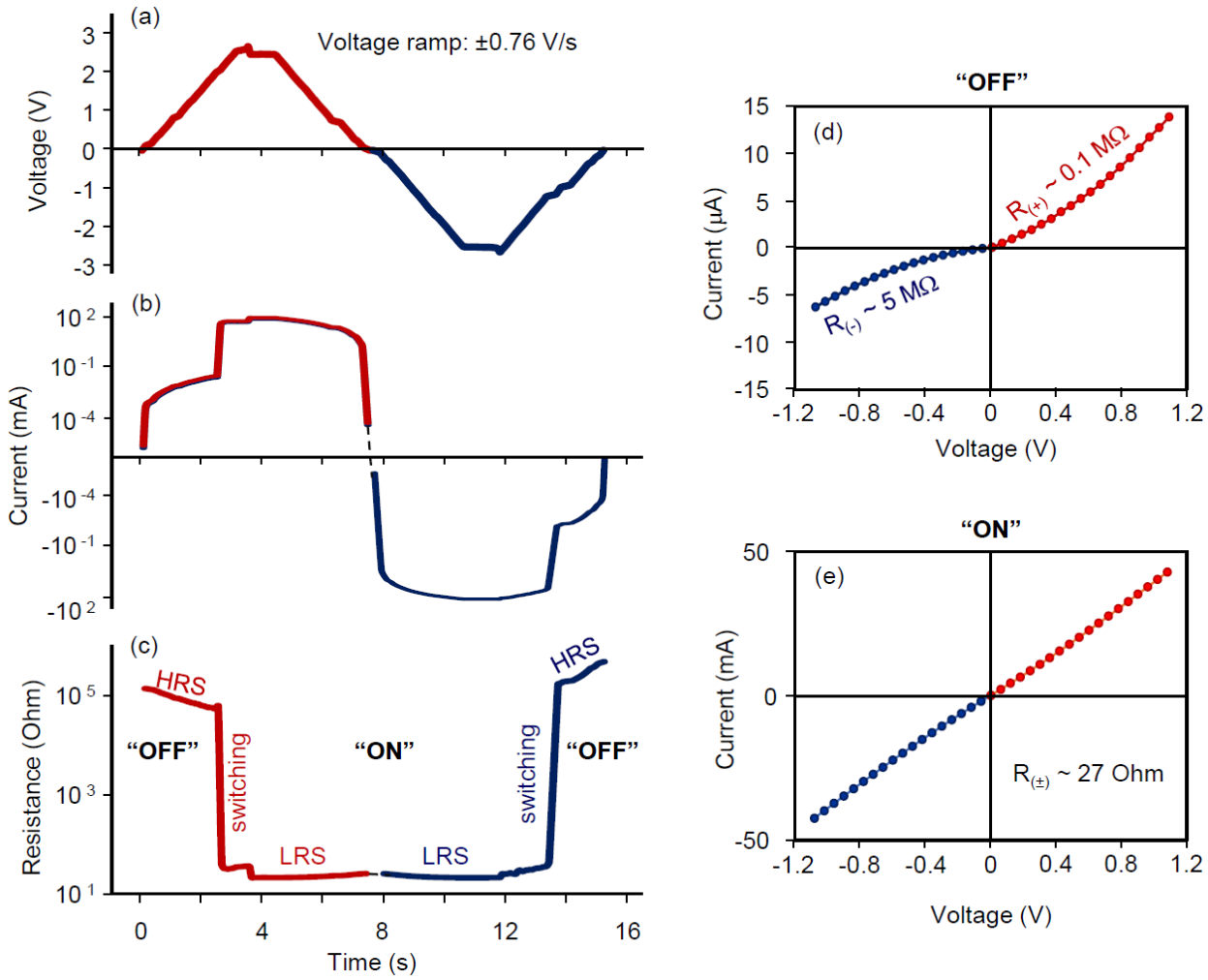

Fig. S13 Characterization of resistive switching in Fe_3O_4 thin films obtained by hydrolytic synthesis: (a) applied voltage signal; (b) electric current response; (c) resistance switching during the characterization cycle; (d-e) low signal voltage-current dependencies in (d) "OFF" and (e) "ON" states .

REFERENCES

S1 Turova, N. Ya; Turevskaya, E. P.; Kessler, V. G.; Yanovskaya, M.I. *The Chemistry of Metal Alkoxide*. Kluwer Academic Publishers, 2002. https://doi.org/10.1007/b113856.

S2 Ismail, H. M. A Thermoanalytic Study of Metal Acetylacetonates. *J. Anal. Appl. Pyrolysis* 1991, 21 (3), 315–326. https://doi.org/10.1016/0165-2370(91)80006-t.

S3 Pinna, N.; Grancharov, S.; Beato, P.; Bonville, P.; Antonietti, M.; Niederberger, M. Magnetite Nanocrystals: Nonaqueous Synthesis, Characterization, and Solubility. *Chem. Mater.* 2005, 17 (11), 3044–3049. https://doi.org/10.1021/cm050060+.

S4 Lalancette, R. A.; Syzdek, D.; Grebowicz, J.; Arslan, E.; Bernal, I. The Thermal Decomposition and Analyses of Metal Tris-Acetylacetonates. *J. Therm. Anal. Calorim.* 2018, 135 (6), 3463–3470. https://doi.org/10.1007/s10973-018-7598-8.

S5 Drozdov, A. S.; Ivanovski, V.; Avnir, D.; Vinogradov, V. V. A Universal Magnetic Ferrofluid: Nanomagnetite Stable Hydrosol with No Added Dispersants and at Neutral PH. *J. Colloid Interface Sci.* 2016, 468, 307–312. https://doi.org/10.1016/j.jcis.2016.01.061.